International Journal of Remote Sensing

ISSN: 0143-1161 (Print) 1366-5901 (Online) Journal homepage: http://www.tandfonline.com/loi/tres20

Extraction of power-transmission lines from vehicle-borne lidar data

Haiyan Guan, Yongtao Yu, Jonathan Li, Zheng Ji & Qi Zhang

To cite this article: Haiyan Guan, Yongtao Yu, Jonathan Li, Zheng Ji & Qi Zhang (2016) Extraction of power-transmission lines from vehicle-borne lidar data, International Journal of Remote Sensing, 37:1, 229-247

To link to this article: http://dx.doi.org/10.1080/01431161.2015.1125549

INTERNATIONAL JOURNAL OF REMOTE SENSING, 2016
VOL. 37, NO. 1, 229–247
http://dx.doi.org/10.1080/01431161.2015.1125549

Taylor & Francis
Taylor & Francis Group

Extraction of power-transmission lines from vehicle-borne lidar data

Haiyan Guan[a], Yongtao Yu[b], Jonathan Li[c,d], Zheng Ji[e] and Qi Zhang[f]

[a]College of Geography and Remote Sensing, Nanjing University of Information Science & Technology, Nanjing, China; [b]Faculty of Computer and Software Engineering, Huaiyin Institute of Technology, Huaian, China; [c]School of Information Science and Engineering, Xiamen University, Xiamen, Fujian, China; [d]Department of Geography and Environment Management, University of Waterloo, Waterloo, Canada; [e]School of Remote Sensing & Information Engineering, Wuhan University, Wuhan, Hubei, China; [f]Public Administration College, Zhejiang Gongshang University, Hangzhou, China

ABSTRACT

This paper presents a step-wise method for extracting power-transmission lines and towers from vehicle-borne light detection and ranging (lidar) data. First, this method estimates road ranges with regard to incidence angles and separates off-road points from road-surface points by applying elevation-difference and slope criteria to the road ranges scan-line by scan-line. Then, three filters, in terms of height, spatial density, and a combination of size and shape, are proposed to extract power-transmission line/power tower points from the identified off-road points, followed by the extraction of individual power-transmission lines via Hough transform and Euclidean distance clustering. Finally, a three-dimensional (3D) power-transmission line is modelled as a horizontal line in the x–y plane and a vertical catenary curve defined by a hyperbolic cosine function in the x–z plane. We evaluated the method using two data sets acquired by the RIEGL VMX-450 system. The average completeness, correctness, and quality of the extracted power-lines on two data sets are 0.92, 0.99, and 0.91, respectively, and the positional accuracies including root mean square error and maximum error averaged 0.07 and 0.05 m, respectively. The results show that the proposed method extracts power-transmission lines from large-scale, vehicle-borne lidar data with good thematic and positional accuracy.

ARTICLE HISTORY
Received 26 February 2015
Accepted 22 November 2015

1. Introduction

As power-transmission lines interconnect various electrical power-generation facilities and distributors of the bulk electricity transmission system, their safety significantly affects our daily lives and industrial activities. Accurately and timely monitoring power-transmission lines for re-engineering transmission lines and identifying possible encroachments is an extremely high priority for utility companies. The purposes of extracting power-transmission lines cover two main aspects: (1) vegetation

CONTACT Haiyan Guan guanhy.nj@nuit.edu.cn College of Geography and Remote Sensing, Nanjing University of Information Science & Technology, 219 Ningliu Road, Nanjing, JS, China 210044

encroachment, which aims to prevent growing vegetation from damaging transmission lines; and (2) estimation of the catenary curve, which is used for estimating the amount of sag (McLaughlin 2006).

Objects, such as trees, buildings, and any other fixtures (e.g. lighting and signalling poles), that approach overhead electricity conductors and power-transmission lines too closely can cause fatal or severe shocks and burns. The minimum safety clearance must be maintained in order to prevent such incidents. Trees must be planted far enough away from the transmission facilities so as not to pose a threat to the facilities, such as swaying into the wires. Trees cannot exceed 3 m in height at maturity. Thus, analysis of tree encroachment is one of the most important applications. As such, the estimation of the amount of sag is also to prevent the contact between the lines and overgrown vegetation that encroaches on the required clearance zone for the lines. If high-voltage power-transmission lines are sagging, they may touch tree branches resulting in the failure of electricity to flow in a circuit, and a flashover discharge (and potential sparking) might occur. The tree becomes an electrified body, resulting in power-line single-phase grounding; even short trips can cause power outages and even serious fire. On average, trees are involved in approximately 30% of all power outages (Consumers Energy 2013). In addition, at the substations, transformers are used to step the voltage down for distribution to commercial and residential users. At the point of use, the energy is transformed to a low voltage. Large electrical motors switching on and off can cause widely varying sags and surges in electrical AC loading. Both sags and surges are the most commonly experienced power quality problems among electronic and computer equipment users (Warkentin-Glenn 2006).

Current traditional technologies that used for power-transmission line extraction include:

(1) Manually operated methods, where utility companies hire electrical linesmen to inspect, monitor, and maintain electrical distribution and overhead power-transmission lines. Field survey methods include pole climbing, foot patrols, or inspection using a vehicle (NYPA 2004). These manual methods are very time consuming, labour intensive, inaccurate, and dangerous.
(2) Aerial video surveillance or multispectral imaging, which is an alternative to overhead power-transmission line monitoring (Junaid et al. 2013). Utility companies use aircraft (such as a small plane, helicopter, or unmanned aerial vehicle (UAV)) to maintain their electric transmission networks over thousands of miles passing through dense forests or terrains. This aerial technology is mainly applied to a wide range of sites, in particularl inaccessible areas (Duller et al. 2001). Through the acquired aerial colour images, infrared images, or videos, the damage status of power-line facilities can be detected (Yamamoto and Yamada 1997; Whitworth et al. 2001; Sun et al. 2006; Yan et al. 2007). However, compared with fieldwork, image-based methods are limited by environmental conditions (e.g. light intensity, weather, and distracting background), camera stability, and image degradation due to camera residual sightline motion (Jones et al., 2001; Golightly and Jones 2003).
(3) Polarimetric radar data, which range from millimetre-wave to long- and medium-wavelength polarimetric synthetic aperture radar (POLSAR) (Ma, Goshi, and Shi

2011; Deng et al. 2011). This technology can work under all-weather and all-day conditions. Most polarimetric detection algorithms are based on the polarimetric scattering characteristics of power-transmission lines. However, these technologies are unreliable because of low signal to clutter ratio (SCR), weak backscattering, and noisy data due to ground return.

(4) Airborne lidar, which has gained popularity in documenting the majority of overhead transmission lines in terms of high accuracy and high density (Kim and Sohn 2010, 2013). This technology uses time-of-flight between the emitted and reflected pulses to record the range and other ancillary information of a distant object. This 'fly-by' data acquisition contributes to large-scale power-transmission line corridors. However, environmental factors, such as occlusions caused by high-rise buildings and other objects, may negatively affect airborne lidar in regard to inspecting power-transmission lines within complex urban areas.

Vehicle-borne lidar (also termed mobile lidar or mobile laser scanning), introduced in 2003, represents a promising means for land-based surveying and mapping because it can produce highly accurate, point clouds of extremely high density, generating digital elevation models (DEMs) with centimetre-level accuracy and >100–300 points m^{-2} resolution (Toth 2009; Guan et al. 2013), while most airborne lidar systems provide only 20 cm-level accuracy and 1–20 points m^{-2} resolution (Young et al. 2010; Lim et al. 2013). Additionally, compared with airborne lidar, vehicle-borne lidar provides a dramatic reduction in price-per-mile because of its 'drive-by' data acquisition ability. Along a corridor, vehicle-borne lidar systems capture (and represent in the form of 3D point clouds) trees, bridges, street lighting poles, buildings, power-transmission lines, and road surface features (e.g. markings, pavement cracks) (Yang et al. 2012a) – virtually anything visible to the naked eye. Thereby, the data collected from a single mission can be reused for multiple tasks without the need for further field visits, resulting in an increase in data reusability and efficiency. More importantly, vehicle-borne lidar systems enable zero-traffic impact data acquisition of road corridors since less congestion occurs at night. Thus, vehicle-borne lidar systems are recognized for their ability, in terms of increased safety, efficiency, and abundant and detailed data, to determine various power-transmission lines' physical parameters (e.g. catenary characteristics and vegetation encroachment distances) and use them for further engineering analysis (Lehtomäki et al. 2010; Kukko et al. 2012; Puente et al. 2013; Williams et al. 2013; Babic et al., 2012).

The algorithms that extract power-transmission lines from point clouds are grouped in two categories: (1) classification and (2) mathematical estimation. In the first category, some machine learning methods, such as support vector machine (SVMs) and random forests (RF), first design and summarize multiple features and then train a set of samples to classify power-transmission lines from 3D point clouds (Clode and Rottensteiner 2005; Kim and Sohn 2010). These algorithms are time consuming because substantial samples are required. In addition, the selection of training samples and features of interest are the other two factors that can influence classification accuracy. Most researchers prefer the second category, where Hough transform and RANSAC (RANdom SAmple Consensus) are widely used for extracting linear objects from 3D point clouds or 2D interpolated range data (Liu et al. 2009; Melzer and Briese 2004). Based on the assumption that power-transmission lines are represented by linear structures in the vertical

view, these geometric approaches have been shown to be computationally efficient in extracting power-transmission lines from the interpolated range data. However, Hough transform does not perform well for complex power-transmission lines, particularly those in close proximity.

In this article, we propose a step-wise algorithm for directly extracting 3D power-transmission lines from vehicle-borne lidar data. First, the algorithm detects kerbs and separates off-road points from road-surface points by applying elevation-difference and slope criteria to vehicle-borne lidar data, scan-line by scan-line. Then, a group of multiple features of power-transmission lines are employed, followed by a spatial density filtering method aimed at isolating power-transmission line points in the identified off-road points. Next, the power-transmission line points are grouped into clusters representing individual power-transmission lines via a Euclidean distance clustering method. Finally, a 3D power-transmission line is modelled as a horizontal line in the x–y plane and a vertical catenary curve defined by a hyperbolic cosine function in the x–z plane (Jwa and Sohn 2012). The proposed algorithm was tested on a set of point clouds acquired by the RIEGL VMX-450 system.

2. Vehicle-borne lidar data

This research uses data collected by the RIEGL VMX-450 system. The system comprises two RIEGL VQ-450 laser scanners, four CCD cameras, and the Applanix POS LV (Position and Orientation System for Land Vehicles) 520 processing system containing two Global Navigation Satellite System (GNSS) antennas, an inertia measurement unit (IMU), and a distance measurement indicator (DMI). Together with the POS computer system (PCS), these components are integrated and fixed within a case and mounted on the vehicle roof. The system uses two rotating-head laser scanners, and thus the data from the two scanners form a slant grid-like pattern. Calculation of the ground coordinates for illuminated objects is termed as 'geo-referencing'. The laser scanner is referenced when its position and orientation relative to the mapping coordinate system is known by a set of navigation systems. The navigation data must be precisely time-stamped for integration, and are used to determine the exact location of the mapping points.

The survey area is Xiamen Island (118° 04′ 04″ E, 24° 26′ 46″ N), part of the city of Xiamen, which is a major city on the southeastern coast of China. The data were acquired on 23 April 2012. In this survey, the mean standard deviation of planimetric accuracy for the left and right laser scanners is 4.2 and 3.3 cm, respectively. The mean standard deviation of vertical accuracy for the two laser scanners is 1.7 and 2.1 cm, respectively.

During this survey, two types of parameter were predefined – mission and scanning parameters – as shown in Table 1. The mission parameter category includes target distance and ground speed. The surveyed road was quite busy, with the average driving speed 30–50 km h^{-1}. Because the buildings (e.g. high-rise residential apartments and commercial buildings) are located along this typical urban road, this survey used 30 m and 30 km h^{-1} for target distance and ground speed, respectively. We also used the default values for all scanning parameters, including scan mode, scan-line start, scan-line end, and increment angle. Dcan-line spacing, point spacing, and average point density are defined by Guan et al. (2015):

Table 1. Mission, scanning, and derived parameters from the survey.

Parameter		Description	Value
Mission	S_G	Vehicle speed	30 km h^{-1}
	T_{Dist}	Target distance	30 m
Scanning	L_{Incre}	Scan-line incremental	0.1143°
	S_s	Scan speed/scan rate	200 lines s^{-1}
	S_{Start}	Scan-line start	0°
	S_{End}	Scan-line end	360°
Derived	L_{Dist}	Scan-line spacing	0.0583 m
	P_{Dist}	Point spacing	0.0598 m
	$P_{Density}$	Average point density	286.44 points m^{-2}

$$L_{Dist} = S_G/S_s, \tag{1}$$

$$P_{Dist} = \tan(L_{Incre}) \times T_{Dist}, \tag{2}$$

$$P_{Density} = 1/(P_{Dist} \times L_{Dist}). \tag{3}$$

L_{Dist} is proportional to S_G and inversely proportional to S_s, indicating that the higher the vehicle's speed, the lower the scan-line spacing in the direction of movement while the higher the scan speed, the higher the scan-line spacing. In a single scan-line, P_{Dist} varies markedly with scan angle and scan count but very little with vehicle speed. The point density for vehicle-borne lidar data is heavily reliant on the nominal distance to the target, where the point spacing is measured as well as the incidence angle. $P_{Density}$ can be also determined by dividing the number of vehicle-borne lidar points on the horizontal plane by the total area. Accordingly, at a vehicle speed of 30 km h^{-1}, the values of L_{Dist}, P_{Dist}, and $P_{Density}$ are estimated as 0.0583, 0.0598, and 286.44 points m^{-2}, respectively. From the survey data, two data sets are selected to verify the proposed power-transmission line extraction method. Data set I has 7.8 million points in a road length of 95 m; data set II contains 8.4 million points covering a road length of 90 m, as shown in Figure 1.

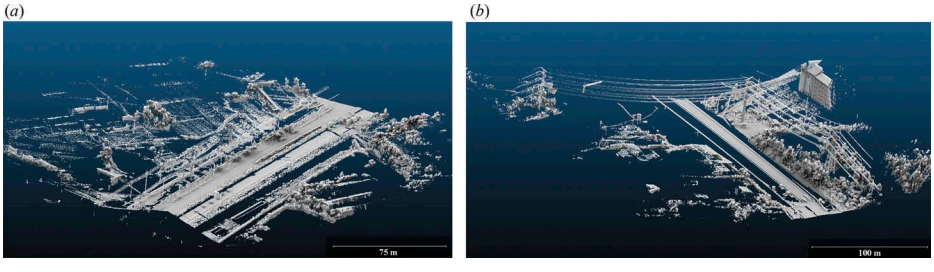

Figure 1. Two RIEGL VMX-450 point cloud data sets: (a) dataset I and (b) data set II (grey: point clouds).

3. Methodology

The proposed algorithm contains the following three steps: (1) off-road point extraction, in which the transverse range of a road is first determined based on incidence angle, and then the separation of off-road from road-surface points is performed based on elevation-difference and slope criteria; (2) power-transmission line extraction, in which three filters, in terms of height, spatial density, and a combination of size and shape, are used to extract individual power-transmission lines; and (3) 3D power-transmission line fitting, in which power-transmission lines are mathematically fitted in the horizontal and vertical planes.

3.1. *Off-road point extraction*

Power towers are normally installed at the sides of roads, and therefore the overhead power-transmission lines are distributed along or transversely to those roads. Moreover, due to the scanning principles of the vehicle-borne lidar system, the point density of the data drops sharply perpendicular to the line of travel, resulting in a large proportion of road-surface points in the data. Therefore, in order to improve the computational efficiency of power-transmission line extraction, separating off-road points from road surface points is performed to cut down the amount of data for processing. In addition, kerbs function not only to contain and direct water flow as part of the drainage system, but also separate road surfaces from sidewalks in an urban environment (Vosselman and Zhou 2009; Serna and Marcotegui 2013; Guan et al. 2014). Kerbs, vertical or nearly vertical to the road surface, are sharp height jumps, and through their detection off-road points can be separated from road surface points.

Each laser scanner in the RIEGL VMX-450 system generates its own 360° 'full circle' profile scans due to the motorized mirror scanning mechanism. The scan angle ranges from −180 to +180°, and the incidence angle is derived by

$$\tan \alpha = D_{\mathrm{h}}/h, \tag{4}$$

where α is the beam incidence angle; h is the sensor elevation from the ground; and D_{h} is the horizontal distance between the scanner and the target of interest. In this study, the system configures two laser scanners at an angle (η) of 45° towards the rear of the vehicle, as shown in Figure 2(a).

The transverse range (D_{t}) from point O to point P'' is estimated by

$$D_{\mathrm{t}} = D_{\mathrm{h}} \cos \eta. \tag{5}$$

Thus, the relation of the incidence angle to the transverse range is represented by

$$\tan \alpha = D_{\mathrm{t}}/h \cos \eta. \tag{6}$$

According to (6), *a priori* knowledge of road width is used to obtain the incidence angle range, $\alpha \in [-K^{\circ}, K^{\circ}]$. The road surface points of interest are within this range, as shown in Figure 2(b).

As mentioned above, point spacing (P_{Dist}) for subsequent points in a scan-line varies markedly with scan angle but very little with vehicle speed. Given that P_{Dist} for all scan-lines is consistent on the ground surface, we extract kerb points scan-line by scan-line

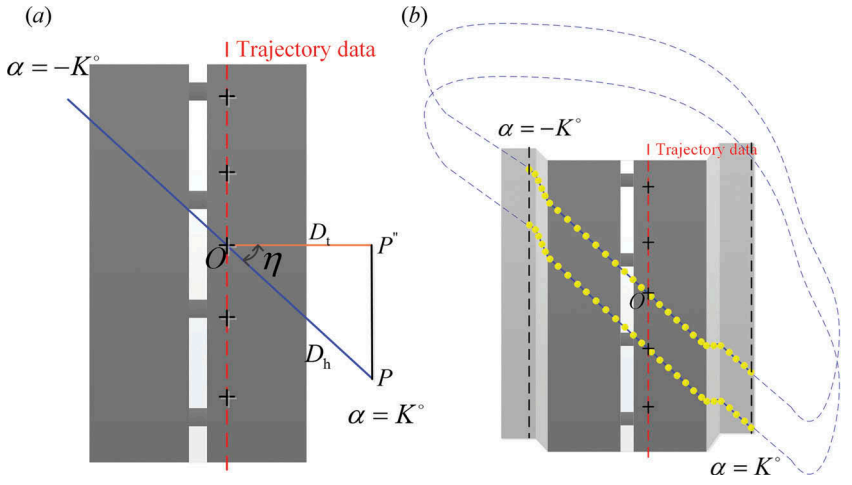

Figure 2. (a) Determination of a transverse range according to incidence angle, and (b) points along each scan-lines within the transverse range.

using two criteria – height difference and slope. Slope at the pavement edge is usually higher than that of consecutive points on the roadway. Moreover, pavement points have higher elevation than adjacent road surface points. The slope criterion detects off-road points, such as cars and kerbs, then the elevation-difference criterion discriminates kerbs from off-road points. Thus, for each scan-line, we mathematically define the slope (S_i) between two consecutive points and the elevation-difference (Z_i) of point $p_i$relative to its adjacent structures as follows:

$$\begin{cases} S_i = \arctan\left(\frac{z_{i+1}-z_i}{\sqrt{(x_{i+1}-x_i)^2+(y_{i+1}-y_i)^2}}\right), \\ Z_i = z_{i+1} - z_i \end{cases} \tag{7}$$

where (x_i, y_i, z_i) and $(x_{i+1}, y_{i+1}, z_{i+1})$ are the coordinates of points p_i and p_{i+1}, respectively. Starting from the point with α = 0°, we subsequently process points in two opposing directions, namely, positive (from 0° to K°) and negative (from –K° to 0°). For each p_i, we define two observations as (Guan et al. 2014):

$$\forall p_i : \begin{cases} if\,(S_i > S_T \,\&\quad (Z_{\min} \le Z_i \le Z_{\max})) & \text{curb candidate} \\ \text{otherwise,} & \text{non-curb point} \end{cases}, \tag{8}$$

where S_T is a given slope threshold, and Z_{min} and Z_{max} are the minimum and maximum thresholds, respectively.

The process of kerb detection can be described as follows: for any point p_i in the pseudo scan-line, if the slope S_i is larger than S_T, as well as elevation-difference G_i in the vicinity being within the range of [Z_{min}, Z_{max}], point p_i is labelled as a kerb candidate; otherwise, p_i will be labelled as a non-kerb point. As the survey vehicle moves along the road, with *a priori* knowledge of the road we select kerb candidates closest to the scanning centre as kerb corners. After identifying all kerb corners from the profiles, we employ a B-spline fitting algorithm to generate two smooth road edges, and finally separate road surface from off-road points.

3.2. *Power-transmission line extraction*

For a vehicle-borne lidar system, point density dramatically decreases perpendicular to the line of travel. After removing road points, which account for a large proportion of vehicle-borne lidar data, it is efficient to use the algorithm of progressive triangulated irregular network (TIN) densification, detailed in Axelsson (2000), to obtain terrain points from off-road points. This TIN densification filtering algorithm is considered to be robust and steady for modelling surfaces with discontinuities such as urban areas (Meng, Currit, and Zhao 2010). The normalized digital surface model (nDSM), a representation of elevated objects on a flat surface, is generated by subtracting the digital terrain model (DTM) from the digital surface model (DSM).

To extract overhead power-transmission lines, three filters regarding data characteristics and objects of interest (e.g. height, spatial density, and a combination of size and shape), and a power-transmission line extractor are applied to the extracted off-road points. For example, overhead power-transmission lines are usually installed at different heights according to different voltages. Along a road, the system can capture at least 75% of a power tower – a cylindrical structure. Relatively speaking, power towers contain highly dense 3D points. The flowchart of the proposed power-transmission line extraction is shown in Figure 3.

(1) Height filter

Every country has its own standards in regard to the design and distribution of power-transmission lines with various types of voltage. For example, according to the National Electrical Safety Code (NESC), vertical clearance to the ground for power-transmission lines of various voltages is given as 6.4 m for 138 kV, 7.0 m for 230 kV, and 8.5 m for 500 kV. However, ground clearance in China is standardized as 5.0 m for 1–10 kV, 10 m for 35–110 kV, and 15 m for 220 kV. Thus, we filter low-rise objects, particularly vegetation fences (such as shrub hedges) that are designed for traffic safety and visual satisfaction, via a height constraint condition (H_{line}):

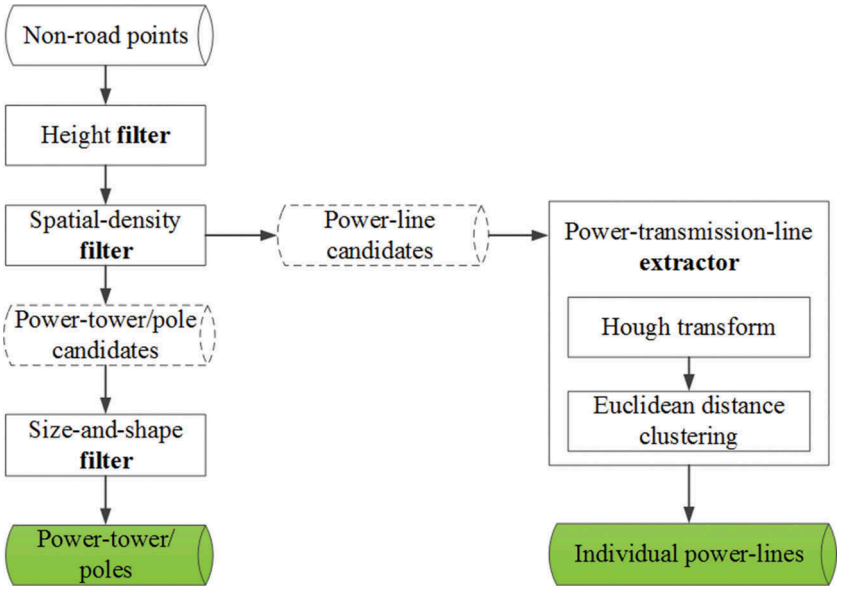

Figure 3. Flowchart of the proposed power-line extraction algorithm.

$$nDSM = (DSM) - (DTM) + H_{\text{line}} \tag{9}$$

(2) Spatial density filter

After filtering out large-scale terrain points and low-rise objects, besides power-transmission lines and towers, high-rise buildings and vegetation are still contained in the off-road point clouds. In addition, occlusions resulting from high-rise buildings and other objects limit the focus in this study to detecting power-transmission lines and power towers/poles along the corridor. Due to the principles of vehicle-borne lidar, vertical building facades and trees have a much higher point density. As a result, we propose two indicators – spatial density and shape-and-size constraints – to remove buildings and vegetation, while simultaneously preserving the power towers/poles.

First, the off-road points are segmented into a number of N voxels with a given voxel size (V_s), as shown in Figure 4. The voxel size depends upon the diameter estimation of power towers. We statistically calculate the number of points (Γ_i) for each voxel ($v_i, i = 0, 1, 2 \ldots N$). In this study, we focus on identifying the locations of power poles, not the power pole details (e.g. conductors and arms). The samples of voxels of power poles are trained to estimate the spatial density threshold (Γ_{pole}). The points within voxel v_i are labelled by the following constraint condition:

$$\forall v_i \begin{cases} \Gamma_i \geq \Gamma_{\text{pole}} & C_{\text{PP}}(\text{power} - \text{pole} \quad \text{candidates}) \\ \text{otherwise}, & C_{\text{PL}}(\text{power} - \text{line} \quad \text{candidates}) \end{cases}. \tag{10}$$

(3) Shape-and-size filter

As a power pole or transmission tower is represented by a cylindrical structure, its shape is approximately a three-quarter circle in the horizontal view while it is a slender rectangle in any arbitrary vertical view. Although the trunk of a tree is similar to a power pole/tower, the tree canopy accounts for a large area in both horizontal and vertical views. In addition, a building facade is linear and rectangular in the horizontal and vertical view, respectively. Thus, region growing is used to subdivide C_{PP} into a number of segments, followed by the size-and-shape filter proposed to extract poles

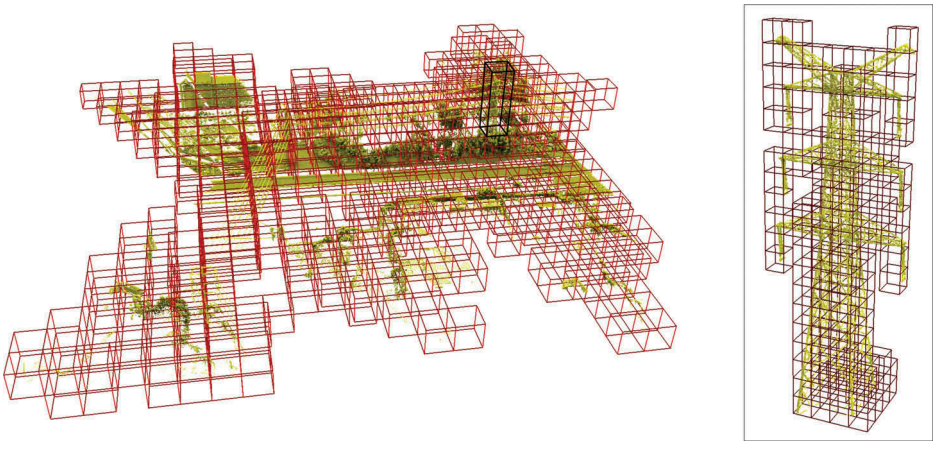

Figure 4. Example of data voxelization. (a) Section of non-road points, and (b) close-up view of a transmission tower.

from segments. Given that buildings are rectangular and linear shape in the vertical and horizontal view, respectively, while pole-like objects appear as elliptical or circular in the horizontal view, the compactness of the polygonal shape can be applied to distinguish buildings and pole-like objects (Yang et al. 2012b). Compactness (S_c) can be calculated by the following equation, proposed by Touya (2007):

$$S_c = 4\pi \frac{C_A}{C_P^2}, \tag{11}$$

where C_A and C_P are the area and perimeter of a cluster, respectively. S_c is 1.0 if the cluster appears circular, while S_c is close to 0.0 if the cluster appears elongated. Thus, according to shape compactness, buildings and pole-like objects can be classified with a given shape threshold, Γ_{shape}.

Considering the sizes of trees and poles, clusters classified as approximately circle-shaped will be eliminated if their size is higher than the threshold (Γ_{size}). The threshold of Γ_{size} is a parameter indicating the diameter of a cluster. Generally, the diameter of power poles in the study area is less than 0.5 m.

(4) Power-transmission line extractoion with Hough transform and Euclidean distance clustering

After removing unwanted structures (e.g. buildings and trees), Hough transform is used to detect power-transmission lines from C_{PL} in the horizontal plane. However, the detected power-transmission lines from the top-down view contain multiple lines. In order to group the classified power-transmission line points into clusters representing separated power-transmission lines, a Euclidean distance clustering method is applied to cluster the power-transmission lines with a predefined clustering distance (Γ_d). Moreover, the detected power-transmission lines in turn facilitate the accurate detection of power poles in C_{PP}.

3.3. *Power-transmission line fitting*

In this section, a fitting method is proposed to respectively project the 3D power-transmission line points onto the *x*–*y* and vertical planes. In the *x*–*y* plane, power-transmission lines can be described by a two-parametric model or one with more than two parameters and additional constraints. This is given by the Hessian normal form (McLaughlin 2006; Levinson and Kane 1993):

$$x\cos\theta + y\sin\theta = \rho, \tag{12}$$

where θ and ρ are the angle between the line's normal vector and the *x*-axis, and the distance between the line and the origin, respectively.

In the vertical plane, a catenary curve, *C*, is fitted in the *x*–*z* plane:

$$z = a + c\cosh\left(\frac{x-b}{c}\right), \tag{13}$$

where *a* and *b* are the parameters for the translation of the origin; and *c* is a scaling factor denoted as the ratio between the tension and the weight of the hanging flexible wire per unit of length. The reconstruction of catenary curves is used to determine the optimal parameters (i.e. *a, b*, and *c*) via a group of segmented power-transmission line points.

4. Experiments and discussion

We tested the proposed power-transmission line extraction algorithm on the two vehicle-borne lidar data sets detailed in Section 2.

4.1. *Power-transmission line extraction*

The two vehicle-borne lidar data sets show typical urban environments with overhanging power-transmission lines, trees, dense shrub hedges, and buildings along roads. According to the information for the road sections studied, the parameters used in this study are empirically selected and are listed in Table 2. *A priori* knowledge of the surveyed road suggested that D_h = 11.70 m and η = 45°. Using the calculated range of incidence angles, ranging from −70 to 70°, all road-surface points were included (see green shading in Figure 5 (a) and (*b*)). Within the calculated incidence angle range, we set S_T = 75°, Z_{min} = 10 cm, and Z_{max} = 30 cm for detecting kerb points scan-line by scan-line. Figure 6 (a) and (b) shows the results of kerb detection. Points shaded red and green belong to the classes kerb and road, respectively. Although certain kerb points (red) were missing because of occlusions caused by cars and other street-scene objects, all road edges were extracted with the assistance of the vehicle trajectory constraint in B-spline cubic interpolation.

Based on the filtering method of the TIN densification filter in Axelsson (2000), the extracted road-edge and off-road points were combined to generate DEM. H_{line} = 3.0 m was used to generate nDSM, according to the power-transmission lines and towers of

Table 2. Parameters used for extracting power-lines.

Processing step	Parameter	Value
Off-road point extraction	Horizontal distance (D_h)	11.7 m
	Scanner configuration angle (η)	45°
	Threshold of slope (S_T)	75°
	Minimum threshold of height difference (Z_{min})	0.1 m
	Maximum threshold of height difference (Z_{max})	0.3 m
Power-line extraction	Height constraint condition (H_{line})	3.0 m
	Voxel size (V_s)	0.5 m
	Threshold of spatial density (Γ_{pole})	200
	Threshold of size (Γ_{size})	0.5 m
	Threshold of shape (Γ_{shape})	0.6
	Clustering distance (Γ_d)	0.3 m

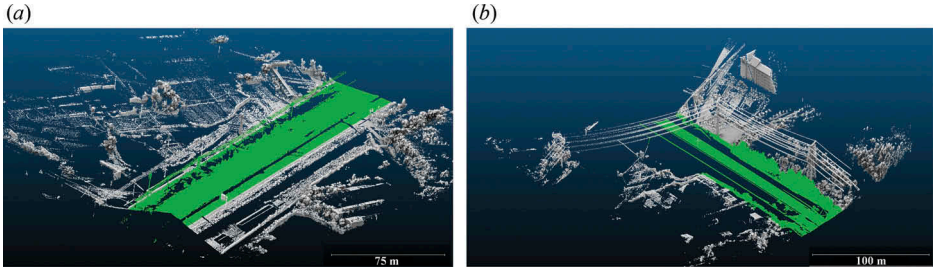

Figure 5. Results of incidence angle based segmentation on (a) data set I, and (b) data set II (green: road surface point candidates ranging from −70 to 70°).

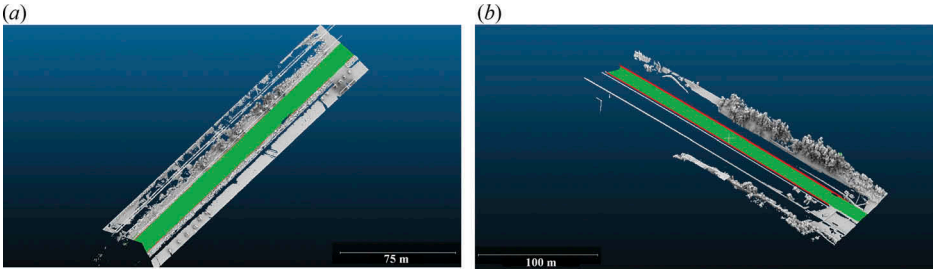

Figure 6. Results of kerb-based road extraction from (a) data set I, and (b) data set II (red: kerb points; green: road surface points; grey: off-road points).

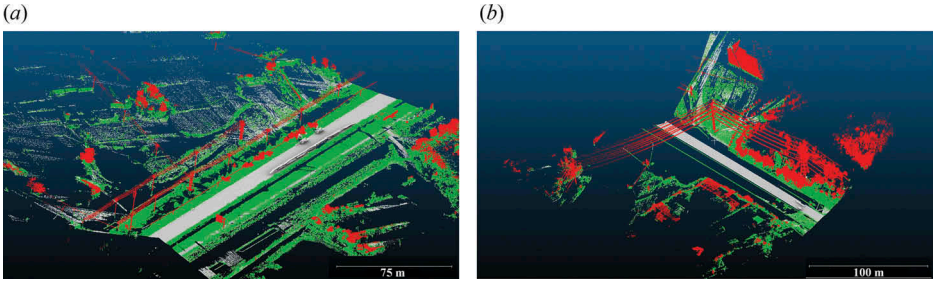

Figure 7. Candidates of power-lines and transmission towers (red) on (a) data set I, and (b) data set II (green: low shrub hedge and tree points; red: filtered points (including power-line points); grey: road surface points).

interest. The areas investigated in this study contain two types of power-transmission line: (1) >138 kV voltage, three-phase transmission lines across the road; and (2) 1–10 kV voltage lines along the road. The power towers for the first type of transmission line are > 30 m, while the power poles supporting the second type of transmission line are around 6 m in height.

In nDSM, the majority of low shrub hedges and trees (green points in Figure 7 (a) and (b)) were removed. The filtered data (red points) include, apart from all power-transmission lines and power towers/poles, tree canopies, high-rise buildings, and other outliers. Without the disturbance of shrub hedges and trees, linear power-transmission lines and cylindrically shaped power towers/poles were easily extracted.

We maintained V_s = 0.5 m to segment the filtered data into a number of voxels, as shown in Figure 8 (a) and (b). A number of samples were selected to statistically obtain the threshold of spatial density Γ_{pole}= 200 to separate the data into the data sets: C_{PP} (including trees, buildings, power poles/towers, and other clustered objects) and C_{PL} (including power-transmission lines, small objects, and outliers). In order to extract power towers/poles from C_{PP}, the values of Γ_{size} and Γ_{shape} were empirically given as 0.5 and 0.6 m, respectively. The power-transmission lines extracted from C_{PL} in turn refined the extracted results of the power towers/poles, as shown in Figure 9 (a) and (b). Several power poles, particularly small ones supporting 1–10 kV transmission lines, were not accurately extracted in Figure 9 (a). The missing power towers/poles cannot separate the long power-transmission lines extracted by Hough transform into small sections. In

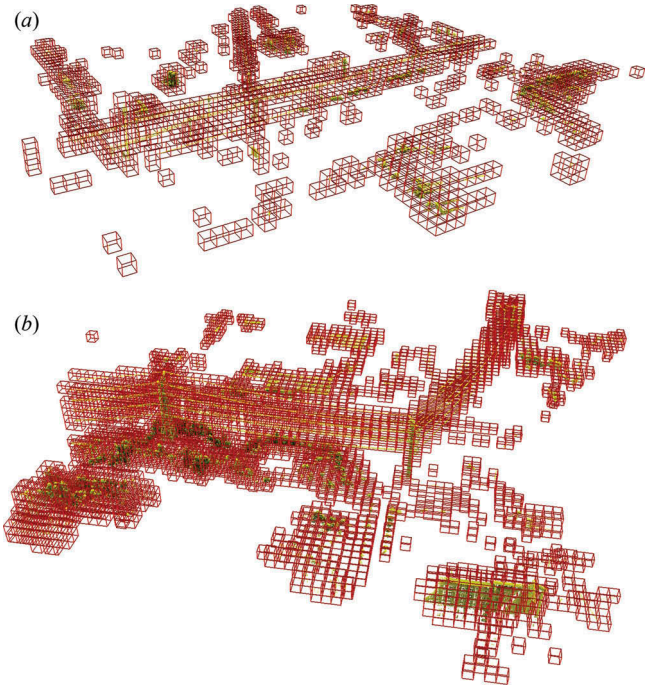

Figure 8. Results of data voxelization on (a) data set I, and (b) data set II (green: lidar points; red: voxels).

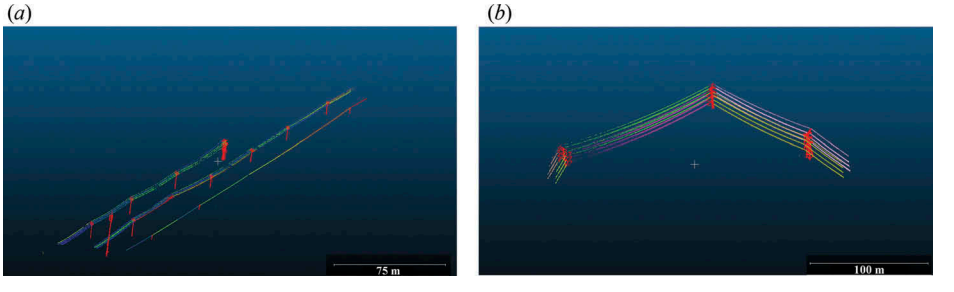

Figure 9. Extracted power-lines along with transmission towers from (a) data set I, and (b) data set II.

general, considering safety factors, the vertical distance between the high-voltage power-transmission lines is designed to be greater than that of low-voltage power-transmission lines. The value of the clustering distance was specified as 0.5 m for individually extracting most of the high-voltage power-transmission lines along the road, as shown in Figure 9 (b).

However, the overhead power-transmission lines across the road were not clustered because of the low point density. For the low-voltage power-transmission lines, we set Γ_d = 0.3 m because their vertical distance is less than 0.5 m. Most of the low-voltage power-transmission lines were individually separated. However, within the rectangle each transmission line section comprising two single lines was clustered into a single

one. This is also because of the characteristics of the low-voltage power-transmission lines, such as small diameter and distances less than 0.3 m. The choice of Γ_d has a major impact on the clustering results. If Γ_d is given a lower value, the points belonging to one power-transmission line are not adequately linked. On the other hand, if Γ_d is given a higher value, the points between different power-transmission lines will be clustered into a single power-transmission line. Γ_d relies on point density, which is further dependent on vehicle speed, scan rate, and the incremental scanning angle, according to Equations (4)–(6).

All the extracted power-transmission lines are fitted in the x–y and x–z planes and modelled in 3D space. As there are too many power-transmission lines to display, and the wires in each group share similar properties of fitting and modelling, a representative of all power-transmission lines is randomly selected and presented in Figure 10. All extracted power-transmission lines are fitted and reconstructed individually in the previous sections. Based on the estimated parameters and functions, a 3D

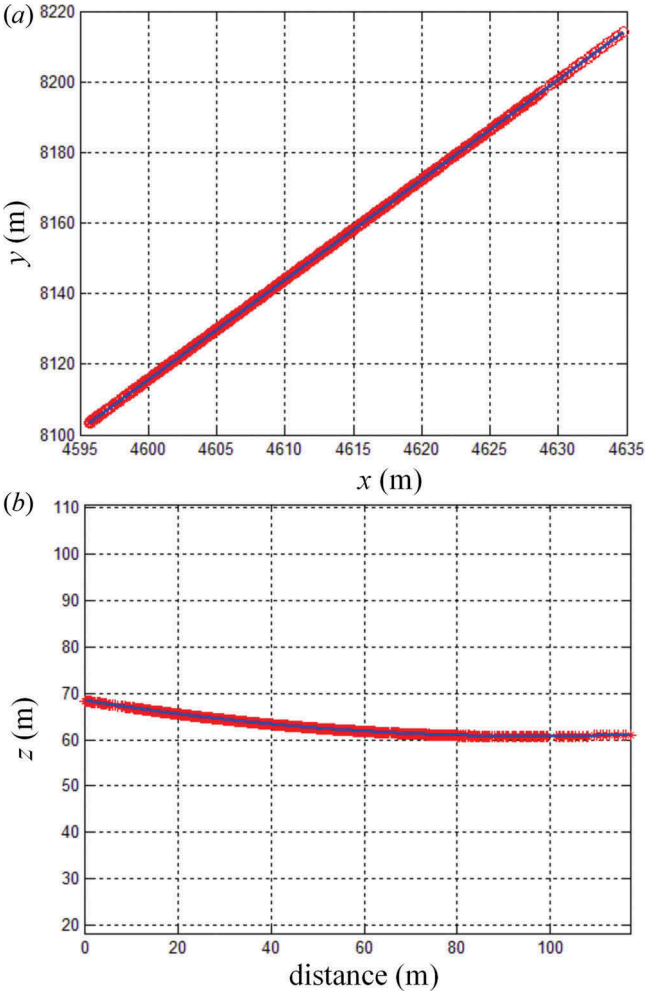

Figure 10. A single fitted catenary power-line on (a) the x–y plane, and (b) the vertical plane.

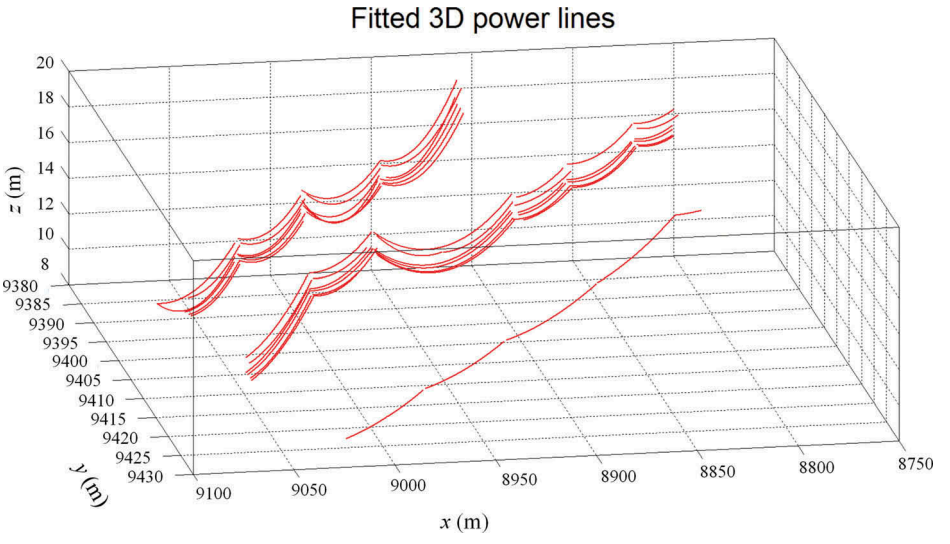

Figure 11. A group of fitted 3D power-lines.

reconstruction map in the study area is shown in Figure 11, where the red lines denote the fitted power-transmission lines of data set I.

4.2. *Quantitative evaluation of power-transmission lines*

In order to validate the applicability of the proposed method, the fitted power-transmission lines were evaluated by two indicators: positional and thematic accuracy. Positional accuracy evaluates the accuracy of the location of the classified power-transmission lines by measuring their distance from their true locations on the ground. Thematic accuracy evaluates the attributes of the classified power-transmission lines by measuring whether their labels are different from their true ones (Congalton and Green 2009). The assessment of thematic accuracy has been widely used by comparing the extracted power-transmission lines with those manually interpolated. Three criteria were used to measure accuracy in this study: completeness, correctness, and quality (Guan et al. 2014). True positives (TP), true negatives (TN), false negatives (FN), and false positives (FP) were counted. TP and TN are respectively the numbers of correctly extracted power-transmission-line points and non-power-transmission-line points that are commonly found in both the reference and the results. FN and FP are respectively the numbers of falsely extracted non-power-transmission-line points and power-transmission-line points that are found only in the results. *Completeness* (E_{cmp}) describes the percentage of TP in the reference data; *Correctness* (E_{crt}) depicts the percentage of TP in the power-transmission-line results; *Quality* (E_{Q}) is an overall measurement. The three criteria are defined as follows:

$$E_{\text{cmp}} = \frac{(\text{TP})}{(\text{TP}) + (\text{FN})}, \tag{14}$$

Table 3. The accuracy of the extracted power-lines.

	Thematic accuracy			Positional accuracy (m)	
Data set	E_{cmp}	E_{crt}	E_Q	D_{MAX}	D_{RMSE}
Data set I	0.93	0.99	0.92	0.07	0.05
Data set II	0.91	0.99	0.91	0.06	0.05
Average	0.92	0.99	0.92	0.07	0.05

$$E_{crt} = \frac{(TP)}{(TP) + (FP)}, \tag{15}$$

$$E_Q = \frac{(TP)}{(TP) + (FN) + (FP)}. \tag{16}$$

The quantitative evaluation results using these three criteria are detailed in Table 3. Our experiments achieved average E_{cmp}, E_{crt}, and E_Q values of 0.92, 0.99, and 0.92, respectively. In regard to thematic accuracy, the E_{cmp} values are lower than the E_{crt} values for the following reasons: (1) power-transmission line points close to the power towers are labelled as power tower points; and (2) in the process of Euclidean distance clustering, some points are excluded when their point spaces are larger than the clustering distance threshold. The selection of the clustering distance threshold plays a significant role in power-transmission line tracking, particularly for those that are quite thin and grouped together or close to each other. Closely spaced power-transmission lines would not be isolated if their vertical distances are higher than the clustering distance threshold; otherwise, the proposed method would miss some points belonging to power-transmission lines if the point space was higher than the clustering distance threshold.

In this study, we also calculated the root mean square error (D_{RMSE}) and maximum error (D_{MAX}) of the distances between points and fitted power-transmission lines to assess the positional accuracy of the extracted lines. The values of D_{RMSE} and D_{MAX} were estimated in both horizontal and vertical space, as shown in Table 3. In our experiments, an average D_{RMSE} value of 0.05 m was achieved. The D_{RMSE} values of distance for the horizontal and vertical spaces of the power-lines match the point density of the collected vehicle-borne lidar data. Point density and data accuracy relate to scanning distance, that is, point density and data accuracy decrease with an increase in scanning distance. Thus, points of power-transmission lines can generate poor positional accuracy. In addition, some points that should belong to power towers may generate the maximum distance in the evaluation of positional accuracy.

5. Conclusions

Power-transmission lines and towers are crucial elements in the positioning of a multitude of bulk electricity transmission systems. Vehicle-borne lidar is opening new possibilities by rapidly collecting highly accurate, geo-referenced spatial data and transforming them into information-rich 3D infrastructure models. We implemented a step-wise method for extracting power-transmission lines from vehicle-borne lidar data. Using the point clouds collected from a RIEGL VMX-450 system, we verified our method

and presented promising results. The thematic and positional accuracy results show that the proposed method is capable of extracting power-transmission lines from vehicle-borne lidar data at high precision. However, the performance of the proposed method is affected to a large extent by the point density of vehicle-borne lidar data. Future research is needed to develop a parameter-free method to decrease the sensitivity of the parameters used in this study to the extracted power-transmission lines.

Disclosure Statement

No potential conflict of interest was reported by the authors.

Funding

This work was supported by the National Natural Science Foundation of China [41301518,41471379,41501501]; and the Natural Science Foundation of Jiangsu Province [BK20151524].

References

Axelsson, P. 2000. "DEM Generation from Laser Scanner Data Using Adaptive TIN Models." *ISPRS Archives* 33 (B4/1) :111–118.

Babic, L., B. Pribicevic, and A. Dapo. 2012. "Mobile Laser Scanning in Transport Infrastructure Documentation and Research." *Ekscentar* 15: 96–99.

Clode, S., and F. Rottensteiner, 2005. "Classification of Trees and Powerlines from Medium Resolution Airborne Laserscanner Data in Urban Environments." *Proceedings of APRS Workshop on Digital Image Computing 2005 (WDIC2005)*, February 21, Brisbane, Australia, pp.97–102.

Congalton, R., and K. Green. 2009. *Assessing the Accuracy of Remotely Sensed Data: Principles and Practices*, 2p. Boca Raton, FL, USA: CRC Press, Taylor & Francis Group, LLC.

Consumers Energy, 2013. "Trees and Power-lines" Retrieved from http://www.consumersenergy.com/content.aspx?id=1592, (last date accessed 15 July 2015).

Deng, S., P. Li, J. Zhang, and J. Yang. 2011. "Power Line Detection from Synthetic Aperture Radar Imagery Using Coherence of Co-Polarisation and Cross-Polarisation Estimated in the Hough Domain." *IET Radar, Sonar & Navigation* 6 (9): 873–880. doi:10.1049/iet-rsn.2011.0332.

Duller, A., C. Whitworth, D. I. Jones, and G. K. Earp. 2001. "Aerial Video Inspection of Overhead Power Lines." *Power Engineering Journal* 15 (1): 25–32. doi:10.1049/pe:20010103.

Golightly, I., and D. Jones. 2003. "Corner Detection and Matching for Visual Tracking during Power Line Inspection." *Image and Vision Computing* 21: 827–840. doi:10.1016/S0262-8856(03)00097-0.

Guan, H., J. Li, Y. Yu, M. Chapman, and C. Wang. 2015. "Automated Road Information Extraction from Mobile Laser Scanning Data." *IEEE Transactions on Intelligent Transportation Systems* 16 (1): 194–205. doi:10.1109/TITS.2014.2328589.

Guan, H., J. Li, Y. Yu, and C. Wang. 2013. *Geometric Validation of a Mobile Laser Scanning System for Urban Applications*. Taiwan: China (Unpaged CD). May 1–3, 2013.

Guan, H., J. Li, Y. Yu, C. Wang, M. Chapman, and B. Yang. 2014. "Using Mobile Laser Scanning Data for Automated Extraction of Road Markings." *ISPRS Journal of Photogrammetry & Remote Sensing* 87: 93–107. doi:10.1016/j.isprsjprs.2013.11.005.

Jones, D. I., and G. K. Earp. 2001. "Camera Sightline Pointing Requirements for Aerial Inspection of Overhead Power Lines." *Electric Power Systems Research* 57: 73–82. doi:10.1016/S0378-7796(01)00100-6.

Junaid, A., A. S. Malik, L. Xia, and N. Ashikin. 2013. "Vegetation Encroachment Monitoring for Transmission Lines Right-of-Ways: A Survey." *Electric Power Systems Research* 95: 339–352. doi:10.1016/j.epsr.2012.07.015.

Jwa, Y., and G. Sohn. 2012. "A Piecewise Catenary Curve Model Growing for 3D Power-Line Reconstruction." *Photogrammetric Engineering & Remote Sensing* 78 (12): 1227–1240. doi:10.14358/PERS.78.11.1227.

Kim, H. B., and G. Sohn. 2010. "3D Classification of Power-Line Scene from Airborne Laser Scanning Data Using Random Forests." *ISPRS Archives* 38 (3A): 126–132.

Kim, H. B., and G. Sohn. 2013. "Point-Based Classification of Power Line Corridor Scene Using Random Forests." *Photogrammetric Engineering & Remote Sensing* 79 (9): 821–833. doi:10.14358/PERS.79.9.821.

Kukko, A., H. Kaartinen, J. Hyyppä, and Y. Chen. 2012. "Multiplatform Approach to Mobile Laser Scanning." *ISPRS Archives* 39 (B5) :484–488.

Lehtomäki, M., A. Jaakkola, J. Hyyppä, A. Kukko, and H. Kaartinen. 2010. "Detection of Vertical Pole-Like Objects in a Road Environment Using Vehicle-Based Laser Scanning Data." *Remote Sensing* 2 (3): 641–664. doi:10.3390/rs2030641.

Levinson, D., and T. Kane. 1993. "A Usable Solution of the Hanging Cable Problem." *Computers & Structures* 46 (5): 821–844. doi:10.1016/0045-7949(93)90145-4.

Lim, S., C. Thatcher, J. Brock, D. Kimbrow, J. Danielson, and B. Reynolds. 2013. "Accuracy Assessment of a Mobile Terrestrial Lidar Survey at Padre Island National Seashore." *International Journal of Remote Sensing* 34 (18): 6355–6366. doi:10.1080/01431161.2013.800658.

Liu, Y., Z. Li, R. Hayward, R. Walker, and H. Jin. 2009. "Classification of Airborne Lidar Intensity Data Using Statistical Analysis and Hough Transform with Application to Power-Line Corridors." In *Proceedings of Digital Image Computing: Techniques and Applications Conference (DICTA 2009)*, Melbourne, December 1–3. IEEE. doi:10.1109/DICTA.2009.83.

Ma, Q., D. Goshi, and Y. Shi. 2011. "An Algorithm for Power Line Detection and Warning Based on a Millimeter-Wave Radar Video." *IEEE Transactions on Image Processing* 20 (12): 3534–3543. doi:10.1109/TIP.2011.2155079.

McLaughlin, R. A. 2006. "Extracting Transmission Lines from Airborne Lidar Data." *IEEE Geoscience & Remote Sensing Letters* 3 (2): 222–226. doi:10.1109/LGRS.2005.863390.

Melzer, T., and C. Briese, 2004. "Extraction and Modelling of Power Lines from ALS Point Clouds, "Proceedings of 28th Workshop of the Austrian Association for Pattern Recognition (AGM), June 2004, Hagenberg, Austria, pp. 47–54.

Meng, X., N. Currit, and K. Zhao. 2010. "Ground Filtering Algorithms for Airborne Lidar Data: A Review of Critical Issues." *Remote Sensing* 2: 833–860. doi:10.3390/rs2030833.

NYPA, 2004. "Vegetation Management Solutions for High-Voltage Transmission Lines." Letter of Energy Currents, New York Power Authority, (last date accessed: 15 June 2014) http://gis.tavanir.org.ir/maghalat/enercur-nypa.pdf

Puente, I., H. González-Jorge, J. Martínez-Sánchez, and P. Arias. 2013. "Review of Mobile Mapping and Surveying Technologies." *Measurement* 46: 2127–2145. doi:10.1016/j.measurement.2013.03.006.

Serna, A., and B. Marcotegui. 2013. "Urban Accessibility Diagnosis from Mobile Laser Scanning Data." *ISPRS Journal of Photogrammetry and Remote Sensing* 84: 23–32. doi:10.1016/j.isprsjprs.2013.07.001.

Sun, C., R. Jones, H. Talbot, X. Wu, K. Cheong, R. Beare, and M. Berman. 2006. "Measuring the Distance of Vegetation from Powerlines Using Stereo Vision." *ISPRS Journal of Photogrammetry and Remote Sensing* 60 (4): 269–283. doi:10.1016/j.isprsjprs.2006.03.004.

Toth, C., 2009. "R&D of Mobile Lidar Mapping and Future Trends, "Proceedings of ASPRS 2009 Annual Conference, Baltimore, Maryland, March 9–13, 2009.

Touya, G. 2007. "A Road Network Selection Process Based on Data Enrichment and Structure Detection." 10th ICA Workshop on Generalization and Multiple Representation, Moscow, August 2–3.

Vosselman, G., and L. Zhou. 2009. "Detection of Kerbstones in Airborne Laser Scanning Data." *ISPRS Archives* 38 (3/W8) :110–116.

Warkentin-Glenn, D. 2006. *Electric Power Industry in Nontechnical Language*. USA: PennWell Books.

Whitworth, C. C., A. Duller, D. Jones, and G. Earp. 2001. "Aerial Video Inspection of Overhead Power-Lines." *Power Engineering Journal* 15 (1): 25–32. doi:10.1049/pe:20010103.

Williams, K., M. Olsen, G. Roe, and C. Glennie. 2013. "Synthesis of Transportation Applications of Mobile Lidar." *Remote Sensing* 5 (9): 4652–4692. doi:10.3390/rs5094652.

Yamamoto, K., and K. Yamada, 1997. "Analysis of the Infrared Images to Detect Power-Lines." Proceedings of IEEE TENCON '97. IEEE Region 10 Annual Conference. Speech and Image Technologies for Computing and Telecommunications. Brisbane, Australia, Dec. 4, pp.343–346.

Yan, G., C. Li, G. Zhou, W. Zhang, and X. Li. 2007. "Automatic Extraction of Power-Lines from Aerial Images." *IEEE Geoscience and Remote Sensing Letters* 4 (3): 387–391. doi:10.1109/LGRS.2007.895714.

Yang, B., L. Fang, Q. Li, and J. Li. 2012a. "Automated Extraction of Road Markings from Mobile Lidar Point Clouds." *Photogrammetric Engineering & Remote Sensing* 78 (4): 331–338. doi:10.14358/PERS.78.4.331.

Yang, B., Z. Wei, Q. Li, and J. Li. 2012b. "Automated Extraction of Street-Scene Objects from Mobile Lidar Point Clouds." *International Journal of Remote Sensing* 33 (18): 5839–5861. doi:10.1080/01431161.2012.674229.

Young, A. P., M. J. Olsen, N. Driscoll, R. E. Flick, R. Gutierrez, R. T. Guza, E. Johnstone, and F. Kuester. 2010. "Comparison of Airborne and Terrestrial Lidar Estimates of Seacliff Erosion in Southern California." *Photogrammetric Engineering & Remote Sensing* 76 (4): 421–427. doi:10.14358/PERS.76.4.421.